Self-consistent Vlasov-Maxwell description of the longitudinal dynamics of intense charged particle beams

Ronald C. Davidson and Edward A. Startsev

Plasma Physics Laboratory, Princeton University, Princeton, New Jersey 08543, USA
(Received 22 December 2003; published 18 February 2004)

This paper describes a self-consistent kinetic model for the longitudinal dynamics of a long, coasting beam propagating in straight (linear) geometry in the z direction in the smooth-focusing approximation. Starting with the three-dimensional Vlasov-Maxwell equations, and integrating over the phase-space $(\mathbf{x}_\perp, \mathbf{p}_\perp)$ transverse to beam propagation, a closed system of equations is obtained for the nonlinear evolution of the longitudinal distribution function $F_b(z, p_z, t)$ and average axial electric field $\langle E_z^s \rangle (z, t)$. The primary assumptions in the present analysis are that the dependence on axial momentum p_z of the distribution function $f_b(\mathbf{x}, \mathbf{p}, t)$ is factorable, and that the transverse beam dynamics remains relatively quiescent (absence of transverse instability or beam mismatch). The analysis is carried out correct to order $k_z^2 r_w^2$ assuming slow axial spatial variations with $k_z^2 r_w^2 \ll 1$, where $k_z \sim \partial/\partial z$ is the inverse length scale of axial variation in the line density $\lambda_b(z, t) = \int dp_z F_b(z, p_z, t)$, and r_w is the radius of the conducting wall (assumed perfectly conducting). A closed expression for the average longitudinal electric field $\langle E_z^s \rangle (z, t)$ in terms of geometric factors, the line density λ_b, and its derivatives $\partial \lambda_b / \partial z, \ldots$ is obtained for the class of bell-shaped density profiles $n_b(r, z, t) = (\lambda_b / \pi r_b^2) f(r/r_b)$, where the shape function $f(r/r_b)$ has the form specified by $f(r/r_b) = (n + 1)(1 - r^2/r_b^2)^n$ for $0 \le r < r_b$, and $f(r/r_b) = 0$ for $r_b < r \le r_w$, where $n = 0, 1, 2, \ldots$. The general kinetic formalism developed here is valid for the entire range of beam intensities (proportional to λ_b) ranging from low-intensity, emittance-dominated beams, to very-high-intensity, low-emittance beams.

PACS numbers: 41.75.–i, 52.59.Sa, 52.35.–g, 52.59.Tb

I. INTRODUCTION

High energy accelerators, transport systems, and storage rings [1–8] have a wide range of applications ranging from basic research in high energy and nuclear physics, to applications such as spallation neutron sources, heavy ion fusion, and nuclear waste transmutation, to mention a few examples. Charged particle beams are subject to various collective processes that can affect the beam quality. Of particular importance at the high beam currents and charge densities of practical interest are the effects of the intense self-fields produced by the beam space charge and current on determining detailed equilibrium, stability, and transport properties. In general, a complete description of collective processes in intense charged particle beams is provided by the three-dimensional Vlasov-Maxwell equations [1] for the self-consistent nonlinear evolution of the beam distribution function, $f_b(\mathbf{x}, \mathbf{p}, t)$, and the self-generated electric and magnetic fields, $\mathbf{E}^s(\mathbf{x}, t)$ and $\mathbf{B}^s(\mathbf{x}, t)$. While considerable progress has been made in analytical and numerical simulation studies of intense beam propagation [9–39], the effects of finite geometry and intense self-fields often make it difficult to obtain detailed predictions of beam equilibrium, stability, and transport properties based on the Vlasov-Maxwell equations. Nonetheless, often with the aid of numerical simulations, there has been considerable recent analytical progress in applying the Vlasov-Maxwell equations to investigate the detailed equilibrium and stability properties of intense charged particle beams. These investigations include a wide variety of

applications ranging from the Harris-type instability driven by large temperature anisotropy with $T_{\perp b} \gg T_{\parallel b}$ [37], to the dipole-mode two-stream instability for an intense ion beam propagating through background electrons [29], to the resistive hose instability [34] and the sausage and hollowing instabilities [35] for intense beam propagation through background plasma, to the development of a nonlinear stability theorem [22,23] in the smooth-focusing approximation.

While the collective processes described in the previous paragraph are three dimensional in nature, considerable theoretical progress has also been made in the development and application of one-dimensional Vlasov-Maxwell models [40–47] to describe the longitudinal beam dynamics for a long coasting beam, with applications ranging from plasma echo excitations to the investigation of coherent soliton structures, both compressional and rarefactive (holelike). Such one-dimensional Vlasov descriptions rely heavily on using a quasi-self-consistent geometric-factor (g-factor) model [46–55] to incorporate the average effects of the transverse beam geometry and the surrounding wall structure. Several limitations are evident in existing g-factor models. First, the models [40–55] typically assume a flattop (step-function) density profile in the plane perpendicular to beam propagation. While this is a good approximation for very-low-emittance, space-charge-dominated beams [1,49–53], the case typically encountered in beams with low-to-moderate intensity is one in which the transverse density profile is bell shaped. Second, with the exception

of the g-factor model for a step-function density profile developed by Reiser *et al.* [50–53], other g-factor models neglect the dependence of the beam edge radius (r_b) and root-mean-square radius (R_b) on the line density λ_b of beam particles, an effect that becomes increasingly important at moderate and high beam intensities. Finally, some one-dimensional Vlasov treatments Taylor expand the field perturbations about the beam axis at $r = 0$, an approximation which is not necessary and has questionable validity, particularly at moderate and high beam intensities.

The purpose of the present paper is to develop an improved one-dimensional kinetic model describing the self-consistent nonlinear evolution of the longitudinal distribution function $F_b(z, p_z, t)$ and average axial electric field $\langle E_z^s \rangle(z, t)$ for a very long charge bunch (coasting beam) propagating through a cylindrical conducting pipe with radius r_w, and confined in the transverse direction by an applied focusing force $\mathbf{F}_{foc}^{tr}$ described in the smooth-focusing approximation. For simplicity, to illustrate the basic approach, in the present analysis the cylindrical pipe is assumed to be perfectly conducting, and the beam transport geometry is assumed to be straight (linear). The analysis can be extended in a straightforward manner to include the effects of a conducting wall with finite resistive and capacitive impedance, as well as the effects of a slip factor η in large-aspect-ratio circular geometry. Extension of the present analysis to incorporate these effects will be the subject of a future publication. In the present analysis, the coasting beam propagates in the z direction with directed axial kinetic energy $(\gamma_b - 1)m_b c^2$, where $\gamma_b = (1 - \beta_b^2)^{-1/2}$ is the relativistic mass factor, $V_b = \beta_b c$ is the average axial velocity of the beam particles, m_b is the rest mass of a beam particle, and c is the speed of light *in vacuo*. Furthermore, the beam dynamics is treated in the thin-beam (paraxial) approximation, and the particle motions in the beam frame are assumed to be nonrelativistic.

For simplicity, the present analysis is carried out in the beam frame where the particle motions are nonrelativistic and the self-generated fields are assumed to have electrostatic polarization ($\nabla \times \mathbf{E}^s = 0$ and $\mathbf{B}^s = 0$). The final results for the longitudinal Vlasov-Maxwell equations are then Lorentz transformed back to the laboratory frame, moving with axial velocity $-V_b = -\beta_b c$ relative to the average motion of the particles in the beam frame.

In Sec. II, the starting point is the fully nonlinear, three-dimensional Vlasov-Maxwell equations for the distribution function $f_b(\mathbf{x}, \mathbf{p}, t)$ and self-generated fields in the beam frame (unprimed variables). A reduced Vlasov equation for the longitudinal distribution function $F_b(z, p_z, t) = \int dx dy \int dp_x dp_y f_b(\mathbf{x}, \mathbf{p}, t)$ is obtained by projecting out (integrating over) the transverse phase-space variables $(\mathbf{x}_\perp, \mathbf{p}_\perp)$. Making the single ansatz so that the dependence of the distribution function $f_b(\mathbf{x}, \mathbf{p}, t)$ on axial momentum p_z is factorable [Eq. (15)] leads to a closed system of equations describing the self-consistent evolution of the longitudinal distribution function $F_b(z, p_z, t)$ and the average axial electric field $\langle E_z^s \rangle(z, t)$. Here, assuming axisymmetry in the transverse plane ($\partial/\partial\theta = 0$), the average $\langle \cdots \rangle$ denotes the weighted transverse spatial average over $n_b(r, z, t)/\lambda_b(z, t)$ defined in Eq. (26), where $n_b = \int d^3 p f_b$ is the number density of beam particles, and $\lambda_b = \int dp_z F_b = \int dx dy n_b$ is the axial line density of beam particles.

In Sec. III, we assume that the beam dynamics is relatively quiescent in the transverse plane (no transverse instability or beam mismatch), and take the transverse density profile to have the fixed-shape form $n_b = (\lambda_b/\pi r_b^2)f(r/r_b)$ where the shape function $f(r/r_b) = (n + 1)(1 - r^2/r_b^2)^n$ for $0 \le r < r_b$, and $f(r/r_b) = 0$ for $r_b < r \le r_w$. Here, $n = 0, 1, 2, \ldots$ is an integer, with $n = 0$ corresponding to a step-function density profile, and r_b is the edge radius of the beam. Moreover, the root-mean-square beam radius $R_b = \langle r^2 \rangle^{1/2}$ and edge radius r_b generally depend on the line density through the radial force-balance condition in Eqs. (33) and (38), respectively. Of course, this dependence is weak ($r_b \simeq$ const) for a low-intensity, emittance-dominated beam, whereas $r_b^2 \propto \lambda_b$ for a very-low-emittance, space-charge-dominated beam. Denoting $\partial/\partial z \sim L_z^{-1} \sim k_z$, we assume slow axial variations of $F_b(z, p_z, t)$ and $\lambda_b(z, t)$ with $k_z^2 r_w^2 \ll 1$. The average electric field $\langle E_z^s \rangle(z, t)$, expressed in terms of $\partial\lambda_b/\partial z$ and higher-order derivatives, together with closed forms for the corresponding geometric factors are calculated self-consistently correct to $0(k_z^2 r_w^2)$ for the class of bell-shaped density profiles with $n = 0, 1, 2, \ldots$ described above. The results show a strong dependence of the geometric factors on profile shape and beam intensity λ_b.

In Sec. IV, as a simple application, the resulting coupled equations for the longitudinal distribution function $F_b(z, p_z, t)$ and the average electric field $\langle E_z^s \rangle(z, t)$ are solved in the linearization approximation for the case of low-to-moderate beam intensity treating $r_b \simeq$ const (independent of λ_b). As expected, the analysis leads to collective oscillations with sound-wave-like characteristics modified by cubic dispersion. The detailed oscillation and damping properties of the perturbation of course depends on the choice of equilibrium distribution function $F_b^0(p_z)$ about which the system is perturbed.

Finally, in Sec. V, the key results derived in the beam frame are transformed back to the laboratory frame to facilitate practical applications of the improved kinetic model of the longitudinal beam dynamics developed here.

II. THEORETICAL MODEL AND ONE-DIMENSIONAL VLASOV EQUATION

The present analysis considers a very long charge bunch (coasting beam) with characteristic axial length

l_b and radius r_b satisfying $l_b \gg r_b$. The coasting beam is made up of particles with charge e_b and rest mass m_b propagating in the z direction with directed axial kinetic energy $(\gamma_b - 1)m_b c^2$, where $\gamma_b = (1 - \beta_b^2)^{-1/2}$ is the relativistic mass factor, $V_b = \beta_b c$ is the average axial velocity of the beam particles, and c is the speed of light *in vacuo*. It is assumed that the beam propagates through a straight, perfectly conducting cylindrical pipe with wall radius r_w, and the applied transverse focusing force $\mathbf{F}_{\text{foc}}^{\text{tr}}$ is modeled in the smooth-focusing approximation. For example, one simple model is $\mathbf{F}_{\text{foc}}^{\text{tr}} = -\gamma_b m_b \omega_{\beta\perp}^2 \mathbf{x}_\perp$, where $\omega_{\beta\perp} = \text{const}$ is the average focusing frequency associated with the applied focusing field, and $\mathbf{x}_\perp$ is the transverse displacement from the cylinder axis. Finally, the nonlinear dynamics of the beam particles is treated in the thin-beam (paraxial) approximation, and the particle motions in the beam frame are assumed to be nonrelativistic [1].

The most general description of the nonlinear collective interactions in an intense charged particle beam is provided by the nonlinear Vlasov-Maxwell equations [1], which is the theoretical framework adopted in the present analysis. For simplicity, the analysis is carried out in the beam frame ($V_b = \beta_b c = 0$ and $\gamma_b = 1$), and the kinetic description is based on the Vlasov-Maxwell equations, which describe the self-consistent nonlinear evolution of the distribution function $f_b(\mathbf{x}, \mathbf{p}, t)$ and the self-generated electric and magnetic fields, $\mathbf{E}^s(\mathbf{x}, t)$ and $\mathbf{B}^s(\mathbf{x}, t)$, in the six-dimensional phase space $(\mathbf{x}, \mathbf{p})$. Here, the (unprimed) variables $(\mathbf{x}, \mathbf{p}, t)$ denote beam-frame variables. For present purposes, the self-generated fields in the beam frame are assumed to have longitudinal polarization (electrostatic approximation) with $\nabla \times \mathbf{E}^s = 0$ and $\mathbf{B}^s = 0$. In this case, the nonlinear Vlasov-Maxwell equations describing the self-consistent nonlinear evolution of $f_b(\mathbf{x}, \mathbf{p}, t)$ and $\mathbf{E}^s(\mathbf{x}, t)$ can be expressed as [1]

$$\frac{\partial f_b}{\partial t} + \mathbf{v} \cdot \frac{\partial f_b}{\partial \mathbf{x}} + (\mathbf{F}_{\text{foc}}^{\text{tr}} + e_b \mathbf{E}^s) \cdot \frac{\partial f_b}{\partial \mathbf{p}} = 0, \qquad (1)$$

and

$$\nabla \cdot \mathbf{E}^s = 4\pi e_b \int d^3 p f_b, \qquad \nabla \times \mathbf{E}^s = 0, \qquad (2)$$

where $\mathbf{v} = \mathbf{p}/m_b$ is the (nonrelativistic) particle velocity in the beam frame. Of course, once the solutions for $f_b(\mathbf{x}, \mathbf{p}, t)$ and $\mathbf{E}^s(\mathbf{x}, t)$ are determined from Eqs. (1) and (2) in the beam frame, the corresponding solutions in the laboratory frame (moving with axial velocity $-V_b \hat{\mathbf{e}}_z$ relative to the beam frame) can be obtained by transforming the phase-space variables and field components to the laboratory frame (primed variables) according to [22]

$$x' = x, \qquad y' = y, \qquad z' = \gamma_b(z + V_b t), \qquad p_x' = p_x,$$
$$p_y' = p_y, \qquad p_z' = \gamma_b(p_z + \gamma m_b V_b),$$
$$t' = \gamma_b(t + V_b z/c^2), \qquad \gamma' = \gamma_b(\gamma + V_b p_z/m_b c^2), \qquad (3)$$

and

$$[E_x^s]' = \gamma_b E_x^s, \qquad [E_y^s]' = \gamma_b E_y^s, \qquad [E_z^s]' = E_z^s,$$
$$[B_x^s]' = -\frac{1}{c}\gamma_b V_b E_y^s, \qquad [B_y^s]' = \frac{1}{c}\gamma_b V_b E_x^s, \qquad (4)$$
$$[B_z^s]' = 0.$$

In Eq. (3), $\gamma' = (1 + \mathbf{p}'^2/m_b^2 c^2)^{1/2}$ and $\gamma = (1 + \mathbf{p}^2/m_b^2 c^2)^{1/2}$ are the kinematic mass factors, and $\gamma \simeq 1 + \mathbf{p}^2/2m_b^2 c^2$ because the particle motions in the beam frame are assumed to be nonrelativistic.

Returning to the beam frame, the Vlasov-Poisson equations (1) and (2) are fully three dimensional and describe the self-consistent nonlinear evolution of the distribution function $f_b(\mathbf{x}, \mathbf{p}, t)$ in the transverse phase space $(\mathbf{x}_\perp, \mathbf{p}_\perp) = (x, y, p_x, p_y)$ and longitudinal phase space (z, p_z). Two macroscopic moments of particular interest for a coasting beam (long charge bunch) are the volume number density $n_b(x, y, z, t)$ and axial line density $\lambda_b(z, t)$ defined by

$$n_b(\mathbf{x}, t) = \int d^3 p f_b(\mathbf{x}, \mathbf{p}, t),$$
$$\lambda_b(z, t) = \int dx dy n_b(\mathbf{x}, t) = \int dx dy \int d^3 p f_b. \qquad (5)$$

Here, $\int dx dy \cdots = \int_0^{r_w} dr r \int_0^{2\pi} d\theta \cdots$ denotes integration over the accessible transverse configuration space extending to the conducting wall located at radius $r = r_w$, $\int d^3 p \cdots = \int_{-\infty}^{\infty} dp_x \int_{-\infty}^{\infty} dp_y \int_{-\infty}^{\infty} dp_z \cdots$ denotes integration over momentum space, and (r, θ, z) are cylindrical polar coordinates with $x = r\cos\theta$ and $y = r\sin\theta$, where $r = (x^2 + y^2)^{1/2}$ is the radial distance from the beam axis at $(x, y) = (0, 0)$. Because the cylindrical wall located at $r = r_w$ is perfectly conducting, the nonlinear Vlasov-Poisson equations are to be solved subject to the boundary conditions

$$[E_z]_{r=r_w} = 0 = [E_\theta]_{r=r_w}. \qquad (6)$$

Moreover, the present analysis, carried out for a long coasting beam, assumes that the distribution function $f_b(\mathbf{x}, \mathbf{p}, t)$ is such that the transverse beam dynamics is relatively quiescent (e.g., no transverse instability), and that there are no particles extending beyond some outer radius $r_0 < r_w$, i.e.,

$$f_b(\mathbf{x}, \mathbf{p}, t) = 0, \quad \text{for } r_0 < r \leq r_w. \qquad (7)$$

That is, there is a well-defined vacuum region outside the beam with zero number density, $n_b = 0$ in the region $r_0 < r \leq r_w$ [see Eqs. (5) and (7)]. Finally, it is assumed that

$$f_b(\mathbf{x}, \mathbf{p}, t) = 0, \quad \text{for } p_x \to \pm\infty,$$
$$p_y \to \pm\infty, \quad \text{or} \quad p_z \to \pm\infty, \qquad (8)$$

which is consistent with the existence of the density integral defined in Eq. (5).

For purposes of deriving a one-dimensional Vlasov equation describing the beam dynamics in the longitudinal phase space (z, p_z), it is convenient to rewrite the three-dimensional Vlasov equation (1) describing the

nonlinear evolution of $f_b(\mathbf{x}, \mathbf{p}, t)$ in the equivalent form

$$\frac{\partial}{\partial t} f_b + v_z \frac{\partial}{\partial z} f_b + \mathbf{v}_\perp \cdot \frac{\partial}{\partial \mathbf{x}_\perp} f_b + (\mathbf{F}_{\text{foc}}^{\text{tr}} + e_b \mathbf{E}_\perp^s) \cdot \frac{\partial}{\partial \mathbf{p}_\perp} f_b$$
$$+ e_b E_z^s \frac{\partial}{\partial p_z} f_b = 0. \qquad (9)$$

Here, $\mathbf{x}_\perp = x \hat{\mathbf{e}}_x + y \hat{\mathbf{e}}_y$ and $\mathbf{p}_\perp = p_x \hat{\mathbf{e}}_x + p_y \hat{\mathbf{e}}_y$ denote the transverse phase-space variables, and $\mathbf{v}_\perp = \mathbf{p}_\perp / m_b$ is the transverse particle velocity. We introduce the transverse projection operator $\langle \cdots \rangle_\perp$ defined by

$$\langle \cdots \rangle_\perp = \int dx dy \int dp_x dp_y \cdots, \qquad (10)$$

where $\int dx dy \cdots = \int_0^{2\pi} d\theta \int_0^{r_w} dr r \cdots$ and $\int dp_x dp_y \cdots = \int_{-\infty}^{\infty} dp_x \int_{-\infty}^{\infty} dp_y \cdots$. Note that the operator defined in Eq. (10) has the effect of projecting out the transverse phase-space coordinates $(\mathbf{x}_\perp, \mathbf{p}_\perp)$. Introducing the longitudinal distribution function $F_b(z, p_z, t)$ defined by

$$F_b(z, p_z, t) = \langle f_b(\mathbf{x}, \mathbf{p}, t) \rangle_\perp$$
$$= \int dx dy \int dp_x dp_y f_b(\mathbf{x}, \mathbf{p}, t), \qquad (11)$$

we operate on Eq. (9) with $\int dx dy \int dp_x dp_y \cdots$. Some straightforward integration by parts that makes use of the boundary conditions in Eqs. (7) and (8) readily gives for the nonlinear evolution of $F_b(z, p_z, t)$

$$\frac{\partial}{\partial t} F_b + v_z \frac{\partial}{\partial z} F_b + e_b \left\langle E_z^s \frac{\partial}{\partial p_z} f_b \right\rangle_\perp = 0. \qquad (12)$$

Note that $E_z^s(\mathbf{x}, t)$ occurs in the average in Eq. (12). We operate on Poisson's equation $\nabla \cdot \mathbf{E}^s = 4\pi e_b \int d^3 p f_b = 4\pi e_b n_b$ in Eq. (2) with $\partial / \partial z$, and make use of $\nabla \times \mathbf{E}^s = 0$ in cylindrical polar coordinates, which gives $\partial E_z^s / \partial r = \partial E_r^s / \partial z$ and $\partial E_\theta^s / \partial z = r^{-1} \partial E_z^s / \partial \theta$. Poisson's equation for $E_z^s(r, \theta, z, t)$ readily becomes

$$\frac{1}{r} \frac{\partial}{\partial r} r \frac{\partial}{\partial r} E_z^s + \frac{\partial^2}{\partial z^2} E_z^s + \frac{1}{r^2} \frac{\partial^2}{\partial \theta^2} E_z^s = 4\pi e_b \frac{\partial}{\partial z} n_b, \quad (13)$$

where $n_b(r, \theta, z, t) = \int d^3 p f_b(r, \theta, z, \mathbf{p}, t)$ is the number density of beam particles. In Eqs. (12) and (13) we note from Eqs. (5) and (11) that the axial line density $\lambda_b(z, t) = \int dx dy n_b = \int dx dy \int d^3 p f_b$ is related (exactly) to the longitudinal distribution function $F_b(z, p_z, t)$ by

$$\lambda_b(z, t) = \int dp_z F_b(z, p_z, t). \qquad (14)$$

The Vlasov equation (12) for the evolution of $F_b(z, p_z, t)$ contains the average $e_b \langle E_z^s \partial f_b \partial p_z \rangle_\perp$ over the three-dimensional distribution function $f_b(\mathbf{x}, \mathbf{p}, t)$. Of course the total distribution function $f_b(\mathbf{x}, \mathbf{p}, t)$ evolves according to the nonlinear Vlasov equation (1), which

generally couples the longitudinal and transverse particle dynamics. As a simplifying ansatz for closure, consistent with the assumption that the transverse beam dynamics remains relatively quiescent, we make the assumption that the dependence of $f_b(\mathbf{x}, \mathbf{p}, t)$ on axial momentum p_z is factorable according to

$$f_b(\mathbf{x}, \mathbf{p}, t) = G_b(\mathbf{x}_\perp, \mathbf{p}_\perp, z, t) F_b(z, p_z, t), \qquad (15)$$

where $G_b(\mathbf{x}_\perp, \mathbf{p}_\perp, z, t)$ and $F_b(z, p_z, t)$ are the transverse and longitudinal distribution functions, respectively. From Eqs. (5), (11), and (15), we readily obtain

$$\int dp_x dp_y G_b(\mathbf{x}_\perp, \mathbf{p}_\perp, z, t) = \frac{n_b(\mathbf{x}, t)}{\lambda_b(z, t)}. \qquad (16)$$

Substituting Eqs. (15) and (16) into the definition of $e_b \langle E_z^s \partial f_b / \partial p_z \rangle_\perp$ then gives

$$e_b \left\langle E_z^s \frac{\partial}{\partial p_z} f_b \right\rangle_\perp = e_b \langle E_z^s \rangle(z, t) \frac{\partial}{\partial p_z} F_b(z, p_z, t), \qquad (17)$$

where the average axial electric field $\langle E_z^s \rangle(z, t)$ is defined by

$$\langle E_z^s \rangle(z, t) \equiv \langle E_z^s(\mathbf{x}, t) G_b(\mathbf{x}_\perp, \mathbf{p}_\perp, z, t) \rangle_\perp$$
$$= \int dx dy E_z^s(\mathbf{x}, t) \frac{n_b(\mathbf{x}, t)}{\lambda_b(z, t)}. \qquad (18)$$

Here, use has been made of the definition of the perpendicular projection operator $\langle \cdots \rangle_\perp$ in Eq. (10). From Eqs. (17) and (18), an important consequence of the factorability ansatz in Eq. (15) is that the average electric field $\langle E_z \rangle(z, t)$ occurring in the longitudinal Vlasov equation (12) corresponds to a transverse spatial average of $E_z^s(\mathbf{x}, t)$ appropriately weighted by the density profile of the beam particles.

In the remainder of this paper we specialize to the case where all beam and field quantities are assumed to be axisymmetric ($\partial / \partial \theta = 0$). Making use of Eqs. (12), (13), and (18), the final set of equations describing the nonlinear evolution of $F_b(z, p_z, t)$ and $\langle E_z^s \rangle(z, t)$ are given by

$$\frac{\partial}{\partial t} F_b + v_z \frac{\partial}{\partial z} F_b + e_b \langle E_z^s \rangle \frac{\partial}{\partial p_z} F_b = 0, \qquad (19)$$

and

$$\langle E_z^s \rangle = 2\pi \int_0^{r_w} dr r \frac{n_b(r, z, t)}{\lambda_b(z, t)} E_z^s(r, z, t). \qquad (20)$$

Here, $E_z^s(r, z, t)$ is determined self-consistently in terms of the density profile $n_b(r, z, t)$ from Poisson's equation (13), which can be expressed as

$$\frac{1}{r} \frac{\partial}{\partial r} r \frac{\partial}{\partial r} E_z^s + \frac{\partial^2}{\partial z^2} E_z^s = 4\pi e_b \frac{\partial}{\partial z} n_b \qquad (21)$$

for $\partial / \partial \theta = 0$. In addition, from Eqs. (5) and (14), the line density $\lambda_b(z, t)$ is related to $F_b(z, p_z, t)$ and $n_b(r, z, t)$ by

$$\lambda_b(z,t) = 2\pi \int_0^{r_w} dr r n_b(r,z,t) = \int dp_z F_b(z,p_z,t). \tag{22}$$

Equations (19)–(22) constitute the final form of the nonlinear Vlasov-Maxwell equations describing the evolution of the longitudinal distribution function $F_b(z,p_z,t)$ and line density $\lambda_b(z,t)$ in a long coasting beam. An important feature is that Eqs. (19)–(22) have been derived for general radial dependence of the density profile $n_b(r,z,t)$. The procedure for the solution is the following. Once the radial dependence of $n_b(r,z,t)$ is specified, $E_z^s(r,z,t)$ is calculated from Poisson's equation (21). The resulting expression for $E_z^s(r,z,t)$ is then substituted into Eq. (20) to determine the average electric field $\langle E_z^s \rangle(z,t)$, which in turn is used in the Vlasov equation (19) to determine the self-consistent nonlinear evolution of $F_b(z,p_z,t)$. Most importantly, the average electric field $\langle E_z^s \rangle(z,t)$ occurring in Eqs. (19) and (20) is appropriately weighted by a transverse spatial average over the density profile of the beam particles. No *a priori* assumption has been made that the density profile corresponds to a flattop (step-function) distribution in the radial direction [40–53]. Nor have we Taylor expanded Poisson's equation (21) about $r = 0$ to estimate the average electric field $\langle E_z^s \rangle(z,t)$ [46,47]. Indeed, Eqs. (19)–(22) are valid for the general choice of the radial density profile and can be applied for arbitrary beam intensity ranging from low-intensity, emittance-dominated beams to very-high-intensity, space-charge-dominated beams.

III. EVALUATION OF AVERAGE LONGITUDINAL FIELD $\langle E_Z^S \rangle$

Equations (19)–(22) constitute the final form of the Vlasov-Maxwell equations describing the nonlinear evolution of the distribution function $F_b(z,p_z,t)$ and line density $\lambda_b(z,t)$. In this section, we make use of Eqs. (20)

and (21) to derive a simplified expression for the average longitudinal electric field $\langle E_z^s \rangle(z,t)$, valid for a wide range of choices of bell-shaped density profiles. For a specified functional form of $n_b(r,z,t)$, Eq. (21) can, of course, be formally solved for $E_z^s(r,z,t)$ using a Green's function method [50,51]. For our purposes here, however, we specialize to the case where the z variation in $E_z^s(r,z,t)$ is slow in comparison with the r variation. In particular, denoting $\partial/\partial z \sim L_z^{-1} \sim k_z$, it is assumed that

$$k_z^2 r_w^2 \ll 1, \tag{23}$$

where r_w is the conducting wall radius.

A. Average electric field $\langle E_z^s \rangle$ for $k_z^2 r_w^2 \ll 1$

Imposing the boundary condition $E_z^s(r = r_w, z, t) = 0$ at the perfecting conducting wall [Eq. (6)], the formal solution to Eq. (21) can be expressed as

$$E_z^s(r,z,t) = -4\pi e_b \int_r^{r_w} \frac{dr}{r} \int_0^r dr r \left(\frac{\partial n_b}{\partial z} - \frac{1}{4\pi e_b} \frac{\partial^2 E_z^s}{\partial z^2} \right), \tag{24}$$

where $n_b(r,z,t)$ is the density profile. The second term on the right-hand side of Eq. (24) is small in comparison with the first term by virtue of the inequality in Eq. (23). Solving iteratively for $E_z^s(r,z,t)$ then gives

$$E_z^s(r,z,t) = -4\pi e_b \int_r^{r_w} \frac{dr}{r} \int_0^r dr r \left(\frac{\partial n_b}{\partial z} + \int_r^{r_w} \frac{dr}{r} \int_0^r dr r \frac{\partial^3 n_b}{\partial z^3} \right) \tag{25}$$

correct to $0(k_z^2 r_w^2)$. Equation (25) is the degree of accuracy used for the longitudinal electric field $E_z^s(r,z,t)$ in the subsequent analysis. Substituting Eq. (25) into Eq. (20) and performing a straightforward integration by parts gives

$$\langle E_z^s \rangle = -2\pi e_b \int_0^{r_w} dr r \frac{n_b}{\lambda_b} \int_r^{r_w} \frac{dr}{r} \left[\frac{\partial}{\partial z} \left(2\pi \int_0^r dr r n_b \right) + \frac{\partial^3}{\partial z^3} \int_0^r dr r \int_r^{r_w} \frac{dr}{r} \left(2\pi \int_0^r dr r n_b \right) \right]$$

$$= -2e_b \int_0^{r_w} \frac{dr}{r} \left(2\pi \int_0^r dr r \frac{n_b}{\lambda_b} \right) \left[\frac{\partial}{\partial z} \left(2\pi \int_0^r dr r n_b \right) + \frac{\partial^3}{\partial z^3} \int_0^r dr r \int_r^{r_w} \frac{dr}{r} \left(2\pi \int_0^r dr r n_b \right) \right]. \tag{26}$$

Equation (26) can be expressed in the equivalent form

$$\langle E_z^s \rangle = \langle E_z^s \rangle^{(1)} + \langle E_z^s \rangle^{(2)}, \tag{27}$$

where $\langle E_z^s \rangle^{(1)}$ and $\langle E_z^s \rangle^{(2)}$ are defined by

$$\langle E_z^s \rangle^{(1)} = -2e_b \int_0^{r_w} \frac{dr}{r} \left(2\pi \int_0^r dr r \frac{n_b}{\lambda_b} \right) \frac{\partial}{\partial z} \left(2\pi \int_0^r dr r \frac{n_b}{\lambda_b} \cdot \lambda_b \right), \tag{28}$$

and

$$\langle E_z^s \rangle^{(2)} = -2e_b \int_0^{r_w} \frac{dr}{r} \left(2\pi \int_0^r dr r \frac{n_b}{\lambda_b} \right) \frac{\partial^3}{\partial z^3} \int_0^r dr r \int_r^{r_w} \frac{dr}{r} \left(2\pi \int_0^r dr r \frac{n_b}{\lambda_b} \cdot \lambda_b \right). \tag{29}$$

Equations (27)–(29) can be used to evaluate a closed expression for $\langle E_z^s \rangle = \langle E_z^s \rangle^{(1)} + \langle E_z^s \rangle^{(2)}$ and the corresponding g

factors for a wide range of choices of beam density profiles $n_b(r, z, t)$. Note from Eqs. (28) and (29) that $\langle E_z^s \rangle^{(2)}$ is of order $k_z^2 r_w^2 \ll 1$ smaller than $\langle E_z^s \rangle^{(1)}$ by virtue of the assumption in Eq. (23).

B. Fixed-shape density profiles $n_b(r, z, t)$

A wide variety of functional forms for the density profile $n_b(r, z, t)$ can be used to evaluate $\langle E_z^s \rangle$ from Eqs. (27)–(29). For example, one approach is to take the transverse distribution function to correspond to the class of matched-beam quasiequilibrium distributions of the form $G_b(H_\perp)$ [1], where $H_\perp = p_\perp^2/2m_b + m_b \omega_{\beta\perp}^2 r^2/2 + e_b \phi$ is the Hamiltonian for transverse particle motion, and ϕ is the space-charge potential determined from Poisson's equation. In this case, the density profile is determined from $n_b/\lambda_b = 2\pi \int_0^\infty dp_\perp p_\perp G_b(H_\perp)$ [Eq. (16)]. For specified functional form of $G_b(H_\perp)$, the radial dependence of the density profile can be determined self-consistently from Poisson's equation $r^{-1}(\partial/\partial r)[r\partial\phi/\partial r] = -4\pi e_b n_b$ for weak variations with axial coordinate z. Depending on the choice of $G_b(H_\perp)$, the radial density profile ranges from a step-function profile for a Kapchinskij-Vladimirskij distribution [1,9–11], to a bell-shaped profile with diffuse radial boundary for a thermal equilibrium distribution [1,2], to a bell-shaped profile with a sharp radial boundary for a waterbag distribution [1,14,15,38]. Whatever the choice of $G_b(H_\perp)$, the mean-square beam radius $R_b^2 = \langle r^2 \rangle \equiv [4\pi^2 \int_0^{r_w} drr^2 \int_0^\infty dp_\perp p_\perp G_b(H_\perp)]/[4\pi^2 \int_0^{r_w} drr \int_0^\infty dp_\perp p_\perp G_b(H_\perp)]$ is determined exactly for a matched beam from the radial force balance equation [1]

$$\omega_{\beta\perp}^2 R_b^2 = \lambda_b \frac{e_b^2}{m_b} + \frac{1}{4} \frac{\tilde{\epsilon}^2}{R_b^2}. \qquad (30)$$

Here, the scaled emittance $\tilde{\epsilon}$ in the beam frame is defined by $\tilde{\epsilon}^2/4R_b^2 = \langle v_\perp^2 \rangle \equiv [4\pi^2 \int_0^{r_w} drr \int_0^\infty dp_\perp p_\perp (p_\perp/m_b)^2 G_b(H_\perp)]/[4\pi^2 \int_0^{r_w} drr \int_0^\infty dp_\perp p_\perp G_b(H_\perp)]$.

The radial force balance equation (30) can be expressed as

$$R_b^4 - R_\lambda^2 R_b^2 - R_\epsilon^4 = 0, \qquad (31)$$

where

$$R_\lambda^2 = \frac{\lambda_b e_b^2}{m_b \omega_{\beta\perp}^2}, \qquad R_\epsilon^4 = \frac{\tilde{\epsilon}^2}{4\omega_{\beta\perp}^2}. \qquad (32)$$

The physically acceptable solution to Eq. (31) is given by

$$R_b^2 = \frac{1}{2}[R_\lambda^2 + (R_\lambda^4 + 4R_\epsilon^4)^{1/2}]. \qquad (33)$$

Note from Eqs. (32) and (33) that the mean-square beam radius R_b^2 depends on the line density λ_b. For a low-intensity emittance-dominated beam with $R_\lambda^2 \ll 2R_\epsilon^2$, Eq. (33) reduces to the familiar result $R_b^2 \simeq R_\epsilon^2 =$

$\tilde{\epsilon}/2\omega_{\beta\perp}$, which is independent of λ_b. On the other hand, for a very-low-emittance, space-charge-dominated beam with $R_\lambda^2 \gg 2R_\epsilon^2$, Eq. (33) reduces to $R_b^2 \simeq R_\lambda^2 = \lambda_b e_b^2/m_b \omega_{\beta\perp}^2$, which is linearly proportional to the line density λ_b. A plot of R_b^2/R_ϵ^2 versus R_λ^2/R_ϵ^2 illustrating this behavior is shown in Fig. 1.

To obtain a closed expression for $\langle E_z^s \rangle$ from Eqs. (27)–(29), for our purposes here we specialize to the class of fixed-shape density profiles $n_b(r, z, t)$ of the form

$$n_b = \begin{cases} \frac{\lambda_b}{\pi r_b^2} f(\frac{r}{r_b}), & 0 \le r < r_b, \\ 0, & r_b < r \le r_w, \end{cases} \qquad (34)$$

where $f(r/r_b)$ is a smooth function that depends on the scaled radial variable r/r_b, and $\lambda_b(z, t) = 2\pi \int_0^{r_w} drr n_b(r, z, t)$ is the line density of beam particles. Note from Eq. (34) that the density profile $n_b(r, z, t)$ has a sharp radial edge at $r = r_b$, and that there is a distinct vacuum region outside the beam ($r_b < r \le r_w$). From $\lambda_b = 2\pi \int_0^{r_w} drr n_b$, we obtain from Eq. (34) the normalization condition

$$\int_0^1 dX X f(X) = \frac{1}{2}. \qquad (35)$$

Similarly, from the definition of mean-square beam radius $R_b^2 = \langle r^2 \rangle = (2\pi \int_0^{r_w} drr^2 n_b)/\lambda_b$, we readily obtain

$$R_b^2 = \eta_b r_b^2, \qquad (36)$$

where the constant η_b is defined by

$$\eta_b = 2 \int_0^1 dX X X^2 f(X). \qquad (37)$$

For specified shape function $f(r/r_b)$, we note from Eqs. (33) and (36) that the edge radius r_b can be expressed as

$$r_b^2 = \frac{1}{2\eta_b}[R_\lambda^2 + (R_\lambda^4 + 4R_\epsilon^4)^{1/2}], \qquad (38)$$
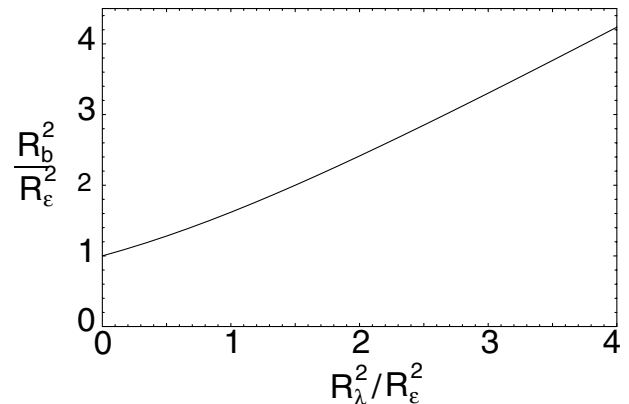

FIG. 1. Plot of R_b^2/R_ϵ^2 versus R_λ^2/R_ϵ^2 obtained from the radial force balance Eq. (33).

where R_λ^2 and R_ϵ^4 are defined in Eq. (32), and the constant η_b is defined in Eq. (37).

There are many practical choices of density shape function $f(r/r_b)$ in Eq. (34). One form of particular interest is the profile

$$f_n\left(\frac{r}{r_b}\right) = (n+1)\left[1 - \frac{r^2}{r_b^2}\right]^n, \qquad 0 \le r < r_b, \quad (39)$$

where $n = 0, 1, 2, \ldots$ is a positive integer, and the normalization of $f_n(r/r_b)$ in Eq. (39) satisfies Eq. (35). For the profile in Eq. (39), we readily obtain from Eq. (37) that

$$\eta_b = \frac{1}{n+2}, \qquad (40)$$

where $n = 0, 1, 2, \ldots$. Here, the root-mean-square beam radius R_b is related to the edge radius r_b by $R_b^2 = \eta_b r_b^2$. The profile shape function $f(r/r_b)$ defined in Eq. (39) gives a wide range of density profile *peakedness*, ranging from a step-function density profile (for $n = 0$) to increasingly peaked profiles (for $n = 1, 2, \ldots$). The two cases corresponding to $n = 0$ and $n = 2$ are illustrated in Fig. 2. For $n = 2$, note from Fig. 2 and Eqs. (34) and (39) that the bell-shaped density profile n_b approaches zero continuously at $r = r_b$ with $[n_b]_{r=r_b} = 0 = [\partial n_b/\partial r]_{r=r_b}$.

We reiterate that the validity of the one-dimensional kinetic model consisting of Eqs. (19), (22), and (26) requires that the beam dynamics remains relatively quiescent in the transverse plane (no transverse instability or beam mismatch). In this regard, it is important to recognize that a sufficient condition for transverse stability of matched-beam quasiequilibrium distributions of the form $G_b(H_\perp)$ is given by $\partial G_b(H_\perp)/\partial H_\perp \le 0$ [see, for example, Chapters 4 and 7 of Ref. [1]]. Here $G_b(H_\perp)$ is the transverse distribution function, $H_\perp = p_\perp^2/2m_b + m_b\omega_{\beta\perp}^2 r^2/2 + e_b\phi(r)$ is the Hamiltonian for transverse particle motion, and ϕ is the space-charge potential. The condition $\partial G_b(H_\perp)/\partial H_\perp \le 0$ assures that there is not
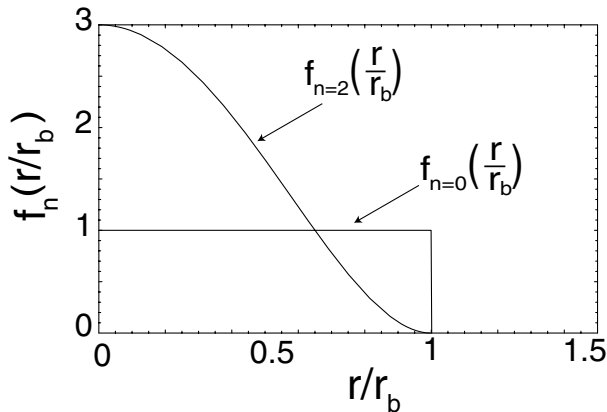

FIG. 2. Shape function profile $f_n(r/r_b)$ defined in Eq. (39) plotted versus r/r_b for $n = 0$ and $n = 2$.

free energy available to drive a collective transverse instability. Finally, for the class of density profiles in Eq. (34), it should be noted that the number density $n_b(r, z, t)$ depends on axial coordinate z through the line density $\lambda_b(z, t)$ and the edge radius $r_b(z, t)$, where $r_b(z, t)$ depends parametrically on $\lambda_b(z, t)$ through Eqs. (32) and (38). We emphasize, however, that the present analysis has been carried out for a long coasting beam and has not been developed for a finite-length charge bunch. Therefore, perturbations in $\lambda_b(z, t)$ are envisioned to be about a constant value of line density $\lambda_{b0} = $ const (independent of z and t).

C. Evaluation of $\langle E_z^s \rangle^{(1)}$ for fixed-shape density profile

We now make use of Eq. (28) to evaluate the leading-order longitudinal electric field $\langle E_z^s \rangle^{(1)}$ for the class of fixed-shape density profiles described by Eq. (34). Because the beam radius r_b generally depends on the line density λ_b [e.g., see Eq. (38)], it is evident from Eqs. (28) and (34) that the radial integrations over n_b/λ_b required in Eq. (28) will also depend on λ_b. Referring to Eq. (28), it is useful to define

$$h_0(\lambda_b) = 2\int_0^{r_w}\frac{dr}{r}\left(2\pi\int_0^r dr r\frac{n_b}{\lambda_b}\right)^2. \qquad (41)$$

It then follows from Eqs. (28) and (41) that

$$\langle E_z^s \rangle^{(1)} = -e_b\left[h_0(\lambda_b)\frac{\partial\lambda_b}{\partial z} + \frac{1}{2}\lambda_b\frac{\partial}{\partial z}h_0(\lambda_b)\right]. \qquad (42)$$

Equation (42) can be expressed in the compact form

$$\langle E_z^s \rangle^{(1)} = -e_b g_0\frac{\partial\lambda_b}{\partial z}, \qquad (43)$$

where the g_0 factor is defined by

$$g_0(\lambda_b) = \frac{1}{2\lambda_b}\frac{\partial}{\partial\lambda_b}[\lambda_b^2 h_0(\lambda_b)], \qquad (44)$$

and $h_0(\lambda_b)$ is defined in Eq. (41).

We now evaluate $h_0(\lambda_b)$ for the class of density profiles described by Eq. (34). Substituting Eq. (34) into Eq. (41) and introducing the dimensionless radial variable $X = r/r_b$ readily gives

$$h_0(\lambda_b) = \ell n\left(\frac{r_w^2}{r_b^2}\right) + 8\int_0^1\frac{dX}{X}\left(\int_0^X dYYf(Y)\right)^2. \qquad (45)$$

For specified profile shape function $f(r/r_b)$, note that the second term on the right-hand side of Eq. (45) is constant (independent of λ_b), whereas the logarithmic term depends on λ_b through the beam radius $r_b(\lambda_b)$ [see Eq. (38)]. Substituting the profile function $f_n(r/r_b) = (n+1)(1 - r^2/r_b^2)^n$, $n = 0, 1, 2, \ldots$, into Eq. (45), we obtain

$$h_0(\lambda_b) = \ell n\left(\frac{r_w^2}{r_b^2}\right) + \alpha_n, \qquad (46)$$

where

$$\alpha_n = \sum_{m=1}^{n+1} \frac{(n+1)}{m(m+n+1)}. \qquad (47)$$

Note from Eq. (47) the sensitive dependence of the constant α_n on the profile shape, ranging from $\alpha_0 = 1/2$ for a step-function density profile ($n = 0$) to $\alpha_1 = 11/12$ for a parabolic profile ($n = 1$), to $\alpha_2 = 73/60$ for $n = 2$, and so on. This, of course, affects the precise values of h_0 [Eq. (46)] and g_0 [Eq. (44)].

Finally, substituting Eq. (46) into Eq. (44), we obtain for the g_0 factor

$$g_0(\lambda_b) = \ell n\left(\frac{r_w^2}{r_b^2}\right) + \alpha_n - \frac{\lambda_b}{2r_b^2}\frac{\partial r_b^2}{\partial \lambda_b}. \qquad (48)$$

Substituting the expression for r_b^2 in Eq. (38) into Eq. (48), we readily obtain

$$g_0(\lambda_b) = \ell n\left(\frac{r_w^2}{r_b^2}\right) + \alpha_n - \frac{1}{2}\frac{R_\lambda^2}{[R_\lambda^4 + 4R_\epsilon^4]^{1/2}}, \qquad (49)$$

where $R_\lambda^2 = \lambda_b e_b^2/m_b\omega_{\beta\perp}^2$ and $R_\epsilon^2 = \tilde{\epsilon}/2\omega_{\beta\perp}$ are defined in Eq. (32). Equation (49) clearly displays the dependence of g_0 on the line density λ_b. For a low-intensity, emittance-dominated beam with $R_\lambda^2 \ll 2R_e^2$, the final term in Eq. (49) is approximately $-R_\lambda^2/4R_\epsilon^2$, which represents a negligibly small correction to $\ell n(r_w^2/r_b^2) + \alpha_n$. On the other hand, for a space-charge-dominated beam with $R_\lambda^2 \gg 2R_\epsilon^2$ the final term in Eq. (49) is approximately $-1/2$, representing a sizable contribution to the g_0 factor. Indeed, for the special case of a step-function density profile ($n = 0$ and $\alpha_0 = 1/2$) the second and third terms on the right-hand side of Eq. (49) exactly cancel in the limit of a space-charge-dominated beam ($R_\lambda^2 \gg 2R_\epsilon^2$), and the g_0 factor is given approximately by $g_0 \simeq \ell n(r_w^2/r_b^2)$ as previously obtained by Reiser *et al.* [52,53]. The expression for $g_0(\lambda_b)$ in Eq. (49), of course, is valid for arbitrary beam intensity and the entire class of fixed-shape density profiles consistent with Eqs. (34) and (39) for $n = 0, 1, 2, \ldots$.

D. Evaluation of $\langle E_z^s \rangle^{(2)}$ for fixed-shape density profile

We now evaluate the second-order electric field $\langle E_z^s \rangle^{(2)}$ defined in Eq. (29) for the class of fixed-shape density profiles described by Eq. (34). As a first example, we consider the case of a low-to-moderate intensity beam ($R_\lambda^2 \ll 2R_\epsilon^2$) where the variation of beam radius r_b with

line density λ_b is treated as negligibly small [see Eq. (38)]. In this case, treating n_b/λ_b as independent of λ_b, Eq. (29) simplifies directly to give

$$\langle E_z^s \rangle^{(2)} = -e_b g_2 r_w^2 \frac{\partial^3 \lambda_b}{\partial z^3}, \qquad (50)$$

where the g_2 factor occurring in Eq. (50) is defined by

$$g_2 = \frac{2}{r_w^2}\int_0^{r_w}\frac{dr}{r}\left(2\pi\int_0^r dr r\frac{n_b}{\lambda_b}\right)\int_0^r dr r\int_r^{r_w}\frac{dr}{r}\left(2\pi\int_0^r dr r\frac{n_b}{\lambda_b}\right). \qquad (51)$$

We substitute Eq. (34) into Eq. (51) with shape function $f_n(r/r_b) = (n+1)(1 - r^2/r_b^2)^n$ specified by Eq. (39) for $0 \leq r < r_b$ and $n = 0, 1, 2, \ldots$. Some straightforward but tedious integration over r in Eq. (51) gives the compact result

$$g_2 = \frac{1}{2}\left[1 - (1 - \beta_n)\frac{r_b^2}{r_w^2} - \frac{1}{n+2}\frac{r_b^2}{r_w^2}\ell n\left(\frac{r_w^2}{r_b^2}\right)\right]. \qquad (52)$$

Here, the constant β_n is defined by

$$\beta_n = \frac{n+1}{n+2} - \sum_{m=1}^{n+1}\frac{1}{m(m+n+2)}, \qquad (53)$$

and r_b^2 is related to the mean-square radius R_b^2 by $R_b^2 = r_b^2/(n+2)$ [see Eqs. (36), (38), and (40)]. It is evident from Eq. (52) that the precise value of the geometric factor g_2 exhibits a sensitive dependence on profile shape. For example, it follows from Eq. (53) that $\beta_0 = 1/6$ for a step-function density profile ($n = 0$), whereas $\beta_1 = 19/60$ for a parabolic density profile ($n = 1$). Furthermore, it follows from Eq. (52) that $g_2 > 0$, with $g_2 \simeq 1/2$ for $r_b^2/r_w^2 \ll 1$ and $g_2 \simeq (1/2)\beta_n$ for $r_b^2/r_w^2 \rightarrow 1$. For the special case of a step-function density profile ($n = 0$), note from Eq. (52) that the g_2 factor is given by

$$g_2 = \frac{1}{2}\left[1 - \frac{5}{6}\frac{r_b^2}{r_w^2} - \frac{1}{2}\frac{r_b^2}{r_w^2}\ell n\left(\frac{r_w^2}{r_b^2}\right)\right]. \qquad (54)$$

Evaluation of $\langle E_z \rangle^{(2)}$ from Eq. (29) for arbitrary beam intensity is somewhat more complicated. For present purposes, we specialize to the case of a step-function density profile ($n = 0$). Substituting Eqs. (34) and (39) into Eq. (29), and carrying out the integrations over r for $n = 0$, we obtain

$$\langle E_z^s \rangle^{(2)} = -\frac{1}{2}e_b r_w^2\left\{\left[1 - \frac{r_b^2}{r_w^2} - \frac{1}{2}\frac{r_b^2}{r_w^2}\ell n\left(\frac{r_w^2}{r_b^2}\right)\right]\frac{\partial^3 \lambda_b}{\partial z^3} - \frac{1}{4}\ell n\left(\frac{r_w^2}{r_b^2}\right)\frac{\partial^3}{\partial z^3}\left(\frac{\lambda_b r_b^2}{r_b^2}\right) - \frac{1}{12}\frac{r_b^4}{r_w^4}\frac{\partial^3}{\partial z^3}\left(\frac{\lambda_b r_w^2}{r_b^2}\right) + \frac{1}{4}\frac{r_b^2}{r_w^2}\frac{\partial^3}{\partial z^3}\left[\lambda_b \ell n\left(\frac{r_w^2}{r_b^2}\right) + \lambda_b\right]\right\}. \qquad (55)$$

Here, for a step-function density profile, r_b^2 depends on λ_b through the force-balance constraint $r_b^2(\lambda_b) = R_\lambda^2 + (R_\lambda^4 + 4R_\epsilon^4)^{1/2}$, where $R_\lambda^2 = \lambda_b e_b^2/m_b\omega_{\beta\perp}^2$ and $R_\epsilon^2 = \tilde{\epsilon}/2\omega_{\beta\perp}$ [see Eqs. (32) and (38) for $n = 0$]. For a general value of beam intensity, note from Eq. (55) that $\langle E_z^s \rangle^{(2)}$ generally has a nonlinear dependence on λ_b and derivatives of λ_b with respect to

TABLE I. Values of the geometric factors g_0 and g_2 for several density profile shapes and low beam intensity ($R_\lambda^2 \ll 2R_\epsilon^2$). Here, $\gamma = 0.5772$ is Euler's constant.

Profile Index n	Normalized profile ($0 \leq r < r_b$) $\frac{\pi r_b^2 n_b}{\lambda_b} = (n+1)(1 - \frac{r^2}{r_b^2})^n$	Geometric factor $g_0 = \ln(\frac{r_w^2}{r_b^2}) + \alpha_n$	Geometric factor $g_2 = \frac{1}{2}[1 - (1 - \beta_n)\frac{r_b^2}{r_w^2} - \frac{1}{n+2}\frac{r_b^2}{r_w^2}\ln(\frac{r_w^2}{r_b^2})]$
0	1	$\ln(\frac{r_w^2}{r_b^2}) + \frac{1}{2}$	$\frac{1}{2}[1 - \frac{5}{6}\frac{r_b^2}{r_w^2} - \frac{1}{2}\frac{r_b^2}{r_w^2}\ln(\frac{r_w^2}{r_b^2})]$
1	$2(1 - \frac{r_w^2}{r_b^2})$	$\ln(\frac{r_w^2}{r_b^2}) + \frac{11}{12}$	$\frac{1}{2}[1 - \frac{41}{60}\frac{r_b^2}{r_w^2} - \frac{1}{3}\frac{r_b^2}{r_w^2}\ln(\frac{r_w^2}{r_b^2})]$
2	$3(1 - \frac{r_w^2}{r_b^2})^2$	$\ln(\frac{r_w^2}{r_b^2}) + \frac{73}{60}$	$\frac{1}{2}[1 - \frac{61}{105}\frac{r_b^2}{r_w^2} - \frac{1}{4}\frac{r_b^2}{r_w^2}\ln(\frac{r_w^2}{r_b^2})]$
3	$4(1 - \frac{r_w^2}{r_b^2})^3$	$\ln(\frac{r_w^2}{r_b^2}) + \frac{1217}{840}$	$\frac{1}{2}[1 - \frac{1279}{2520}\frac{r_b^2}{r_w^2} - \frac{1}{5}\frac{r_b^2}{r_w^2}\ln(\frac{r_w^2}{r_b^2})]$
∞	$\frac{r_b^2}{R_b^2}\exp(-\frac{r^2}{R_b^2})$	$\ln(\frac{r_w^2}{2R_b^2}) + \gamma$	$\frac{1}{2}[1 - (1 + \gamma)\frac{R_b^2}{r_w^2} - \frac{R_b^2}{r_w^2}\ln(\frac{r_w^2}{2R_b^2})]$

z. Indeed, Eq. (55) can generally be expressed in the form

$$\langle E_z^s \rangle^{(2)} = -e_b r_w^2 \left\{ \tilde{g}_2 \frac{\partial^3 \lambda_b}{\partial z^3} + \tilde{g}_3 \left(\frac{\partial \lambda_b}{\partial z}\right)^3 + \tilde{g}_4 \frac{\partial \lambda_b}{\partial z}\frac{\partial^2 \lambda_b}{\partial z^2} \right\}, \tag{56}$$

where the coefficients $\tilde{g}_2$, $\tilde{g}_3$, and $\tilde{g}_4$ depend on λ_b, $\partial r_b^2/\partial \lambda_b$, etc.

In the limit of a low-intensity beam ($R_\lambda^2 \ll 2R_\epsilon^2$), where $r_b^2 \simeq 2R_\epsilon^2 = $ const (independent of λ_b), Eqs. (55) and (56) give the expected result

$$\tilde{g}_2 = g_2, \qquad \tilde{g}_3 = 0, \qquad \tilde{g}_4 = 0, \tag{57}$$

where the geometric factor g_2 is defined in Eq. (54) for a step-function density profile. In this case, Eq. (56) reduces to $\langle E_z^s \rangle^{(2)} = -e_b r_w^2 g_2 \partial^3 \lambda_b/\partial z^3$. On the other hand, for a high-intensity, space-charge dominated beam ($R_\lambda^2 \gg 2R_\epsilon^2$), it follows that $r_b^2 \simeq 2R_\lambda^2$, and the coefficients $\tilde{g}_2$, $\tilde{g}_3$, and $\tilde{g}_4$ in Eq. (56) can be approximated by

$$\tilde{g}_2 = \frac{1}{8}\left[4\left(1 - \frac{r_b^2}{r_w^2}\right) - 3\frac{r_b^2}{r_w^2}\ell n\left(\frac{r_w^2}{r_b^2}\right)\right], \qquad \tilde{g}_3 = \frac{r_b^2}{8\lambda_b^2 r_w^2},$$

$$\tilde{g}_4 = -\frac{3r_b^2}{8\lambda_b r_w^2}\left[1 + 2\ell n\left(\frac{r_w^2}{r_b^2}\right)\right]. \tag{58}$$

Equations (55)–(58) clearly display the strong dependence of $\langle E_z^s \rangle^{(2)}$ on line density λ_b.

To conclude this section, Table I shows the values of the geometric factors g_0 and g_2 obtained from Eqs. (49) and (52) for several density profile shapes. Here, a low-intensity beam ($R_\lambda^2 \ll 2R_\epsilon^2$) has been assumed with $r_b^2 \simeq$ const (independent of λ_b).

Finally, it is important to recognize that the longitudinal dynamics considered in the present paper is assumed to be much slower than the transverse dynamics. Indeed, the longitudinal dynamics in the long-wavelength approximation considered here has characteristic frequency $\omega_\parallel \sim (k_z r_b)\omega_{pb}$ (in the beam frame), where $\omega_{pb} = (4\pi n_b e_b^2/m_b)^{1/2}$ is the plasma frequency, whereas the transverse dynamics has characteristic frequency $\omega_\perp \sim \omega_{\beta\perp} \gtrsim \omega_{pb}$. Since, $k_x^2 r_b^2 \ll 1$ is assumed [see

Eq. (23)], it therefore follows that $\omega_\parallel \ll \omega_\perp$. Hence, in the long-wavelength approximation we can separate the two time scales. The transverse dynamics has enough time to come to a quasiequilibrium which depends parametrically on longitudinal quantities. In this case there is a self-consistent separation of the longitudinal dynamics from the transverse beam dynamics.

IV. LONGITUDINAL VLASOV-MAXWELL EQUATIONS FOR A LOW-INTENSITY BEAM

In Secs. II and III, we provided a systematic derivation of the longitudinal Vlasov-Maxwell equations and associated g factors, valid for a wide range of beam intensity and choice of transverse density profiles. In this section, we specialize to the low-intensity regime ($R_\lambda^2 \ll 2R_\epsilon^2$) where the dependence of the beam radius r_b on line density λ_b can be neglected. In this case, making use of Eqs. (19), (43), (49), (50), and (52), the Vlasov-Maxwell equations describing the evolution of the longitudinal beam distribution $F_b(z, p_z, t)$ and line density $\lambda_b(z, t) = \int_{-\infty}^{\infty} dp_z F_b(z, p_z, t)$ can be expressed as

$$\frac{\partial F_b}{\partial t} + v_z \frac{\partial F_b}{\partial z} + e_b \langle E_z^s \rangle \frac{\partial F_b}{\partial p_z} = 0, \tag{59}$$

where

$$e_b \langle E_z^s \rangle = -e_b^2 g_0 \frac{\partial \lambda_b}{\partial z} - e_b^2 g_2 r_w^2 \frac{\partial^3 \lambda_b}{\partial z^3}. \tag{60}$$

Here, the geometric factors g_0 and g_2 are defined by

$$g_0 = \ell n\left(\frac{r_w^2}{r_b^2}\right) + \alpha_n, \tag{61}$$

$$g_2 = \frac{1}{2}\left[1 - (1 - \beta_n)\frac{r_b^2}{r_w^2} - \frac{1}{n+2}\frac{r_b^2}{r_w^2}\ell n\left(\frac{r_w^2}{r_b^2}\right)\right]. \tag{62}$$

The constants α_n and β_n are defined in Eqs. (47) and (53) for $n = 0, 1, 2, \ldots$, and the transverse density profile assumed in deriving Eqs. (59)–(62) is specified by Eq. (43)

with profile shape function $f_n(r/r_b) = (n+1)(1 - r^2/r_b^2)^n$ for $0 \leq r < r_b$.

Equations (59)–(62) can be used to investigate detailed linear and nonlinear properties of the self-consistent evolution of the beam distribution function $F_b(z, p_z, t)$ and average self-generated electric field $\langle E_z^s \rangle(z, t)$ for a wide range of system parameters and choices of initial distribution function. For our purposes here, we summarize the key stability properties obtained from a linear stability analysis of Eqs. (59) and (60). Perturbations are assumed to be about a spatially uniform $(\partial/\partial z = 0)$ coasting beam with equilibrium distribution function $F_b^0(p_z)$ and normalization $\int_{-\infty}^{\infty} dp_z F_b^0(p_z) = \lambda_{b0}$, where $\lambda_{b0} = \text{const}$ is the unperturbed line density. Substituting $F_b(z, p_z, t) = F_b^0(p_z) + \delta F_b(z, p_z, t)$ and $\lambda_b(z, t) = \lambda_{b0} + \delta\lambda_b(z, t)$ into Eqs. (59) and (60), and retaining terms linear in the perturbation amplitude, we obtain

$$\left(\frac{\partial}{\partial t} + v_z \frac{\partial}{\partial z}\right)\delta F_b = -e_b \delta\langle E_z^s \rangle \frac{\partial}{\partial p_z} F_b^0(p_z), \qquad (63)$$

$$e_b \delta\langle E_z^s \rangle = -e_b^2 g_0 \frac{\partial}{\partial z} \delta\lambda_b - e_b^2 g_2 r_w^2 \frac{\partial^3}{\partial z^3} \delta\lambda_b, \qquad (64)$$

where

$$\delta\lambda_b = \int_{-\infty}^{\infty} dp_z \delta F_b(z, p_z, t). \qquad (65)$$

For present purposes, the perturbations in Eqs. (63)–(65) are taken to be of the form

$$\delta\psi(z, t) = \delta\hat{\psi} \exp(ik_z z - i\omega t), \qquad (66)$$

where k_z is the axial wave number, and ω is the complex oscillation frequency, with $\text{Im}\,\omega > 0$ corresponding to instability (temporal growth). Making use of $\partial/\partial t \to -i\omega$ and $\partial/\partial z \to ik_z$, Eqs. (63) and (64) can be combined to give

$$\delta F_b = -k_z(e_b^2 g_0 - e_b^2 g_2 k_z^2 r_w^2) \frac{\partial F_b^0/\partial p_z}{\omega - k_z v_z} \delta\lambda_b, \qquad (67)$$

which relates the perturbed distribution function δF_b to the perturbed line density $\delta\lambda_b$. It is convenient to introduce effective sound speeds u_{b0} and u_{b2} associated with the geometric factors g_0 and g_1 defined by

$$u_{b0}^2 = \frac{g_0 e_b^2 \lambda_{b0}}{m_b}, \qquad u_{b2}^2 = \frac{g_2 e_b^2 \lambda_{b0}}{m_b}. \qquad (68)$$

Substituting Eqs. (67) and (68) into Eq. (65) then gives

$$D(k_z, \omega)\delta\lambda_b = 0, \qquad (69)$$

where the dielectric function $D(k_z, \omega)$ is defined by

$$D(k_z, \omega) = 1 + k_z(u_{b0}^2 - k_z^2 r_w^2 u_{b2}^2)\frac{m_b}{\lambda_{b0}} \int_{-\infty}^{\infty} dp_z \frac{\partial F_b^0/\partial p_z}{\omega - k_z v_z} \qquad (70)$$

for a nontrivial solution to Eq. (69) with $\delta\lambda_b \neq 0$; note that $D(k_z, \omega) = 0$ plays the role of a dispersion relation that determines the complex oscillation frequency ω in terms of k_z and properties of the equilibrium distribution function $F_b^0(p_z)$. Introducing the distribution function $f_b^0(p_z) \equiv \lambda_{b0}^{-1} F_b^0(p_z)$ normalized according to $\int_{-\infty}^{\infty} dp_z f_b^0(p_z) = 1$, and integrating by parts with respect to p_z in Eq. (70) using $\partial v_z/\partial p_z = 1/m_b$, the dispersion relation $D(k_z, \omega) = 0$ is readily expressed in the compact form

$$D(k_z, \omega) = 1 - k_z^2(u_{b0}^2 - k_z^2 r_w^2 u_{b2}^2) \int_{-\infty}^{\infty} \frac{dp_z f_b^0(p_z)}{(\omega - k_z v_z)^2} = 0. \qquad (71)$$

The dispersion relation (71) can be used to calculate the complex oscillation frequency ω for a wide range of choices of beam distribution function $f_b^0(p_z)$ [1]. It is convenient to introduce the effective susceptibility $\chi(k_z, \omega)$ with dimensions (frequency)$^{-2}$ defined by

$$\chi(k_z, \omega) = \int_{-\infty}^{\infty} \frac{dp_z f_b^0(p_z)}{(\omega - k_z v_z)^2}. \qquad (72)$$

The resulting expressions for $\chi(k_z, \omega)$ are displayed in Table II for various choices of distribution function $f_b^0(p_z)$ ranging from a cold distribution function (entry No. 1) to a Maxwellian distribution (entry No. 5). In Table II, the constant u_T is the effective thermal speed, which is a measure of the velocity spread of the distribution function $f_b^0(p_z)$. For the Maxwellian distribution in Table II (entry No. 5), the plasma dispersion function $Z(\xi)$ is defined by [1]

$$Z(\xi) = \frac{1}{\sqrt{\pi}} \int_{-\infty}^{\infty} du \frac{\exp(-u^2)}{u - \xi}, \qquad (73)$$

where $\xi = \omega/k_z u_T$ is the normalized phase velocity. Equations (71) and (72) and Table II can be used to determine detailed wave propagation properties for several choices of beam distribution functions $f_b^0(p_z)$. For example, for the choice of waterbag (step-function) distribution in entry No. 2, Eqs. (71) and (72) give the dispersion relation

TABLE II. Susceptibility $\chi(k_z, \omega)$ [Eq. (72)] for various choices of $f_b^0(p_z)$.

Entry No.	Distribution $f_b^0(p_z)$	Susceptibility $\chi(k_z, \omega)$ [Eq. (72)]
1	$\delta(p_z)$	$\frac{1}{\omega^2}$
2	$f_b^0 = \begin{cases} \frac{1}{2m_b v_T}, & |p_z| < m_b v_T \\ 0, & |p_z| > m_b v_T \end{cases}$	$\frac{1}{(\omega^2 - k_z^2 v_T^2)}$
3	$\frac{m_b v_T}{\pi} \frac{1}{p_z^2 + m_b^2 v_T^2}$	$\frac{1}{(\omega + i|k_z|v_T)^2}$
4	$\frac{2(m_b v_T)^3}{\pi} \frac{1}{(p_z^2 + m_b^2 v_T^2)^2}$	$\frac{1}{(\omega + i|k_z|v_T)^2}[1 + \frac{2i|k_z|v_T}{\omega + i|k_z|v_T}]$
5	$\frac{1}{m_b v_T} \exp(-\frac{p_z^2}{m_b^2 v_T^2})$	$-\frac{2}{k_z^2 v_T^2}[1 + \xi Z(\xi)]$

$$\omega^2 = k_z^2(u_{b0}^2 + u_T^2 - k_z^2 r_w^2 u_{b2}^2). \qquad (74)$$

Because $k_z^2 r_w^2 \ll 1$ has been assumed [Eq. (23)], the final term in Eq. (74) represents a small correction. Representing $\omega = \omega_r + i\omega_i$ where $\omega_r = \text{Re}\,\omega$ and $\omega_i = \text{Im}\,\omega$, it is clear from Eq. (74) that the solutions are purely oscillatory with

$$\text{Re}\,\omega = \omega_r = \pm k_z(u_{b0}^2 + u_T^2)^{1/2}\left(1 - \frac{1}{2}k_z^2 r_w^2 \frac{u_{b2}^2}{u_{b0}^2 + u_T^2}\right),$$

$$\text{Im}\,\omega = \omega_i = 0. \qquad (75)$$

The solution in Eq. (75) corresponds to forward-moving ($\omega_r/k_z > 0$) and backward-moving ($\omega_r/k_z < 0$) sound-like waves propagating with constant speed $(u_{b0}^2 + u_T^2)^{1/2}$ in the beam frame, with weak cubic dispersive corrections (the term proportional to $u_{b2}^2 k_z^3$). Although the cubic dispersive corrections in Eq. (75) are small, it is precisely this effect that can lead to Korteveg-deVries–like solitons in a weakly nonlinear treatment of the nonlinear beam dynamics [56].

As a second example, we consider the Lorentzian distribution in entry No. 3 of Table II. Substituting the corresponding expression for $\chi(k_z, \omega)$ into Eq. (71), we obtain the dispersion relation

$$(\omega + i|k_z|u_T)^2 = k_z^2(u_{b0}^2 - k_z^2 r_w^2 u_{b2}^2). \qquad (76)$$

In this case, the solutions to Eq. (76) for $k_z^2 r_w^2 \ll 1$ can be expressed as

$$\text{Re}\,\omega = \omega_r = \pm k_z u_{b0}\left(1 - \frac{1}{2}k_z^2 r_w^2 \frac{u_{b2}^2}{u_{b0}^2}\right),$$

$$\text{Im}\,\omega = \omega_i = -|k_z|u_T. \qquad (77)$$

Because $\text{Im}\,\omega = -|k_z|u_T < 0$, we note from Eq. (77) that the wave perturbation is damped due to resonant wave-particle interactions (classical Landau damping) for the choice of Lorentzian distribution function in Table II. This damping is weak ($|\omega_i/\omega_r| \ll 1$) whenever the effective thermal speed u_T is small in comparison with the signal speed u_{b0}, and the damping is strong ($|\omega_i/\omega_r| \gtrsim 1$) whenever $u_T/u_{b0} \gtrsim 1$.

Detailed linear stability properties can, of course, be calculated for other choices of the distribution function in Table II. The main point of this section is that the longitudinal Vlasov-Maxwell equations (59) and (60) are rich in physics content, even at the linearization (small-signal) level. We defer further discussion of Eqs. (59) and (60) to a future publication in which detailed nonlinear properties are discussed.

V. TRANSFORMED EQUATIONS IN THE LABORATORY FRAME

The analysis in Secs. II, III, and IV was carried out in the beam frame (unprimed variables) where $\nabla \times \mathbf{E}^s = 0$.

The transformation of the key results back to the laboratory frame (primed variables) moving with axial velocity $-V_b = -\beta_b c$ relative to the beam frame is readily accomplished according to the transformation in Eqs. (3) and (4). Without presenting algebraic details, the resulting Vlasov equation for the longitudinal distribution function $F_b'(z', p_z', t')$ in the laboratory frame is given by

$$\frac{\partial}{\partial t'}F_b' + v_z'\frac{\partial}{\partial z'}F_b' + e_b\langle E_z^{s'}\rangle'\frac{\partial}{\partial p_z'}F_b' = 0. \qquad (78)$$

Here, the average longitudinal electric field $\langle E_z^{s'}\rangle'(z', t')$ in the laboratory frame is also readily expressed in terms of geometric factors $\partial \lambda_b'/\partial z'$ and higher-order derivatives of the laboratory-frame line density $\lambda_b'(z', t') = \int dp_z' F_b'(z', p_z', t')$. One key modification in the laboratory frame occurs in the radial force balance equation (30), which is replaced by

$$\omega_{\beta\perp}'^2 R_b'^2 = \frac{\lambda_b' e_b^2}{\gamma_b^3 m_b} + \frac{1}{4}\frac{\tilde{\epsilon}'^2}{R_b'^2}, \qquad (79)$$

where $\tilde{\epsilon}'^2/4R_b'^2 = \langle v_\perp'^2\rangle'$. In Eq. (79), $\gamma_b m_b$ is the transverse mass, and the additional factor $1/\gamma_b^2 = 1 - \beta_b^2$ corresponds to a reduction in the space-charge force (the term proportional to $-\beta_b^2$) due to the self-magnetic field $B_\theta^{s'} = -\beta_b E_r^{s'}$ in the laboratory frame. Equation (79) readily gives [1] [compare with Eqs. (32) and (33)]

$$R_b'^2 = \frac{1}{2}[R_\lambda'^2 + (R_\lambda'^4 + 4R_\epsilon'^4)^{1/2}], \qquad (80)$$

where $R_\lambda'^2$ and $R_\epsilon'^4$ are defined by

$$R_\lambda'^2 = \frac{\lambda_b' e_b^2}{\gamma_b^3 m_b \omega_{\beta\perp}'^2}, \qquad R_\epsilon'^4 = \frac{\tilde{\epsilon}'^2}{4\omega_{\beta\perp}'^2}. \qquad (81)$$

Furthermore, the edge radius $r_b'(\lambda_b')$ in the laboratory frame is determined from

$$\eta_b r_b'^2 = R_b'^2 \qquad (82)$$

for the class of fixed-shape density profiles in Eqs. (34) and (39), where $\eta_b = 1/(n + 2)$ is defined in Eq. (40) for $n = 0, 1, 2, \ldots$.

Finally, in the laboratory frame, some straightforward algebra shows that the formal expressions for the average longitudinal electric field $\langle E_z^{s'}\rangle'(z', t')$ in Eqs. (9), (26), and (28) are modified with the replacements $n_b \to n_b'/\gamma_b$, $\lambda_b \to \lambda_b'/\gamma_b$, and $\partial/\partial z \to \gamma_b^{-1}\partial/\partial z'$. For example, Eq. (43) is modified to become

$$\langle E_z^{s'}\rangle'^{(1)} = -e_b g_0' \frac{\partial \lambda_b'}{\partial z'}, \qquad (83)$$

where the laboratory-frame geometric factor $g_0'(\lambda_b')$ is defined by

$$g_0' = \frac{1}{\gamma_b^2}g_0(\lambda_b'). \qquad (84)$$

Here, $g_0(\lambda_b')$ is defined in Eq. (44) [or Eq. (49)] with the

obvious replacements $(r_b, R_\lambda, R_\epsilon, \lambda_b) \rightarrow (r_b', R_\lambda', R_\epsilon', \lambda_b')$. Similarly, in the laboratory frame, for low-to-moderate beam intensity, the second-order electric field in Eq. (50) is modified to become

$$\langle E_z^{s'} \rangle^{\prime(2)} = -e_b g_2' r_w^2 \frac{\partial^3 \lambda_b'}{\partial z'^3}, \tag{85}$$

where the geometric factor g_2' is defined by

$$g_2' = \frac{1}{\gamma_b^4} g_2, \tag{86}$$

and g_2 is defined in Eqs. (51)–(53). Similarly, for arbitrary beam intensity, the second-order electric field in the laboratory frame has the same form as in Eq. (56) with the right-hand side of Eq. (56) scaled by $1/\gamma_b^4$, and λ_b and $\partial/\partial z$ replaced by primed variables.

In concluding this section, it should be emphasized that the detailed theoretical analysis was relatively straightforward to carry out in the beam frame. The key results in the laboratory frame were then readily obtained by Lorentz transformation back to the laboratory frame.

VI. CONCLUSIONS

The purpose of the present paper was to develop an improved one-dimensional kinetic model describing the self-consistent nonlinear evolution of the longitudinal distribution function and average axial electric field $\langle E_z^s \rangle(z, t)$ for a very long charge bunch (coasting beam) propagating through a cylindrical conducting pipe with radius r_w, and confined in the transverse direction by an applied focusing force $\mathbf{F}_{\text{foc}}^{\text{tr}}$ described in the smooth-focusing approximation. For simplicity, to illustrate the basic approach, in the present analysis the cylindrical pipe was assumed to be perfectly conducting, and the beam transport geometry was assumed to be straight (linear). As discussed in Sec. II, the starting point was the fully nonlinear, three-dimensional Vlasov-Maxwell equations for the distribution function $f_b(\mathbf{x}, \mathbf{p}, t)$ and self-generated fields in the beam frame (unprimed variables). A reduced Vlasov equation for the longitudinal distribution function $F_b(z, p_z, t) = \int dx dy \int dp_x dp_y f_b(\mathbf{x}, \mathbf{p}, t)$ was obtained by integrating over the transverse phase-space variables $(\mathbf{x}_\perp, \mathbf{p}_\perp)$. Making the single ansatz that the dependence of the distribution function $f_b(\mathbf{x}, \mathbf{p}, t)$ on axial momentum p_z is factorable, led to a closed system of equations describing the self-consistent evolution of the longitudinal distribution function $F_b(z, p_z, t)$ and the average axial electric field $\langle E_z^s \rangle(z, t)$. Here, assuming axisymmetry in the transverse plane $(\partial/\partial\theta = 0)$, the average $\langle \cdots \rangle$ denotes the weighted transverse spatial average over $n_b(r, z, t)/\lambda_b(z, t)$ defined in Eq. (26), where $n_b = \int d^3 p f_b$ is the number density of beam particles, and $\lambda_b = \int dp_z F_b = \int dx dy n_b$ is the axial line density of beam particles. In Sec. III, we assumed that the beam dynamics was relatively quiescent in the transverse plane (no transverse instability or beam mismatch), and

took the transverse density profile to have the fixed-shape form $n_b = (\lambda_b/\pi r_b^2) f(r/r_b)$, where the shape function $f(r/r_b) = (n + 1)(1 - r^2/r_b^2)^n$ for $0 \le r < r_b$, and $f(r/r_b) = 0$ for $r_b < r \le r_w$. Here, $n = 0, 1, 2, \ldots$ is an integer, with $n = 0$ corresponding to a step-function density profile, and r_b is the edge radius of the beam. Moreover, the root-mean-square beam radius $R_b = \langle r^2 \rangle^{1/2}$ and edge radius r_b generally depend on the line density through the radial force-balance condition in Eqs. (33) and (38), respectively. Of course, this dependence is weak ($r_b \simeq \text{const}$) for a low-intensity, emittance-dominated beam, whereas $r_b^2 \propto \lambda_b$ for a very-low-emittance, space-charge-dominated beam. Denoting $\partial/\partial z \sim L_z^{-1} \sim k_z$, we assumed slow axial variations of $F_b(z, p_z, t)$ and $\lambda_b(z, t)$ with $k_z^2 r_w^2 \ll 1$. The average electric field $\langle E_z^s \rangle(z, t)$, expressed in terms of $\partial\lambda_b/\partial z$ and higher-order derivatives, together with closed forms for the corresponding geometric factors were then calculated self-consistently in Sec. IV correct to $0(k_z^2 r_w^2)$ for the class of bell-shaped density profiles with $n = 0, 1, 2, \ldots$, described above. The results showed a strong dependence of the geometric factors on profile shape and beam intensity λ_b.

In Sec. IV, as a simple application, the resulting coupled equations for the longitudinal distribution function $f_b(z, p_z, t)$ and the average electric field $\langle E_z^s \rangle(z, t)$ were solved in the linearization approximation for the case of low-to-moderate beam intensity treating $r_b \simeq \text{const}$ (independent of λ_b). As expected, the analysis led to collective oscillations with sound-wave-like characteristics modified by cubic dispersion. The detailed oscillation and damping properties of the perturbation, of course, depended on the choice of equilibrium distribution function $F_b^0(p_z)$ about which the system is perturbed. Finally, in Sec. V, the key results derived in the beam frame were transformed back to the laboratory frame to facilitate practical applications of the kinetic model of the longitudinal beam dynamics developed here.

In conclusion, the present analysis has developed an improved one-dimensional kinetic model describing the nonlinear evolution of the longitudinal distribution function $F_b(z, p_z, t)$ and average electric field $\langle E_z^s \rangle(z, t)$. The analysis has been carried out for arbitrary beam intensity and general density profile shape, leading to important generalizations of previous g-factor models [see Eqs. (43)–(45), (50), and (51)]. Since the longitudinal beam dynamics typically depends in detail on the precise values and degree of nonlinearity of the g factors, it is expected that the new results presented here will have several key applications.

In future investigations, the kinetic model for the longitudinal beam dynamics developed here will be applied to various investigations, including the nonlinear Korteweg-deVries–like evolution of axial disturbances and the self-consistent generation of compressional solitons [56].

——————

[1] R. C. Davidson and H. Qin, *Physics of Intense Charged Particle Beams in High Energy Accelerators* (World Scientific, Singapore, 2001), and references therein.

[2] M. Reiser, *Theory and Design of Charged Particle Beams* (Wiley, New York, 1994).

[3] J. D. Lawson, *The Physics of Charged-Particle Beams* (Oxford Science Publications, New York, 1988).

[4] A. W. Chao, *Physics of Collective Beam Instabilities in High Energy Accelerators* (Wiley, New York, 1993).

[5] D. A. Edwards and M. J. Syphers, *An Introduction to the Physics of High-Energy Accelerators* (Wiley, New York, 1993).

[6] T. P. Wangler, *Principles of RF Linear Accelerators* (Wiley, New York, 1998).

[7] See, for example, *Proceedings of the 2001 Particle Accelerator Conference* (IEEE Catalog No. 01CH37268, 2001), pp. 1–4098.

[8] See, for example, *Proceedings of the 1999 International Heavy Ion Fusion Symposium* [Nucl. Instrum. Methods Phys. Res., Sect. A **464**, 1 (2001)].

[9] I. M. Kapchinskij and V. V. Vladimirskij, in *Proceedings of the International Conference on High Energy Accelerators and Instrumentation* (CERN Scientific Information Service, Geneva, 1959), p. 274.

[10] R. L. Gluckstern, in *Proceedings of the 1970 Proton Linear Accelerator Conference, Batavia, IL*, edited by M. R. Tracy (National Accelerator Laboratory, Batavia, IL, 1971), p. 811.

[11] T.-S. Wang and I. Smith, Part. Accel. **12**, 247 (1982).

[12] J. Hofmann, L. J. Laslett, L. Smith, and I. Haber, Part. Accel. **13**, 145 (1983).

[13] J. Struckmeier, J. Klabunde, and M. Reiser, Part. Accel. **15**, 47 (1984).

[14] I. Hofmann and J. Struckmeier, Part. Accel. **21**, 69 (1987).

[15] J. Struckmeier and I. Hofmann, Part. Accel. **39**, 219 (1992).

[16] R. L. Gluckstern, W.-H. Cheng, and H. Ye, Phys. Rev. Lett. **75**, 2835 (1995).

[17] N. Brown and M. Reiser, Phys. Plasmas **2**, 965 (1995).

[18] C. Chen and R. C. Davidson, Phys. Rev. E **49**, 5679 (1994).

[19] C. Chen, R. Pakter, and R. C. Davidson, Phys. Rev. Lett. **79**, 225 (1997).

[20] R. C. Davidson and C. Chen, Part. Accel. **59**, 175 (1998).

[21] R. C. Davidson, W. W. Lee, and P. Stoltz, Phys. Plasmas **5**, 279 (1998).

[22] R. C. Davidson, Phys. Rev. Lett. **81**, 991 (1998).

[23] R. C. Davidson, Phys. Plasmas **5**, 3459 (1998).

[24] R. C. Davidson and H. Qin, Phys. Rev. ST Accel. Beams **2**, 114401 (1999).

[25] P. Stoltz, R. C. Davidson, and W. W. Lee, Phys. Plasmas **6**, 298 (1999).

[26] H. Qin, R. C. Davidson, and W. W. Lee, Phys. Rev. ST Accel. Beams **3**, 084401 (2000); **3**, 109901 (2000).

[27] Q. Qian, W. W. Lee, and R. C. Davidson, Phys. Plasmas **4**, 1915 (1997).

[28] A. Friedman, D. P. Grote, and I. Haber, Phys. Fluids B **4**, 2203 (1992).

[29] R. C. Davidson, H. Qin, P. Stoltz, and T.-S. Wang, Phys. Rev. ST Accel. Beams **2**, 054401 (1999).

[30] J. Haber, A. Friedman, D. P. Grote, S. M. Lund, and R. A. Kishek, Phys. Plasmas **6**, 2254 (1999).

[31] R. A. Kishek, P. G. O'Shea, and M. Reiser, Phys. Rev. Lett. **85**, 4514 (2000).

[32] R. C. Davidson, H. Qin, and P. J. Channell, Phys. Rev. ST Accel. Beams **2**, 074401 (1999); **3**, 029901 (2000).

[33] P. J. Channell, Phys. Plasmas **6**, 982 (1999).

[34] H. S. Uhm and R. C. Davidson, Phys. Rev. ST Accel. Beams **6**, 034204 (2003).

[35] H. S. Uhm, R. C. Davidson, and I. Kaganovich, Phys. Plasmas **8**, 4637 (2001).

[36] R. C. Davidson and H. Qin, Phys. Rev. ST Accel. Beams **4**, 104401 (2001).

[37] E. A. Startsev, R. C. Davidson, and H. Qin, Phys. Plasmas **9**, 3138 (2002).

[38] E. A. Startsev and R. C. Davidson, Phys. Rev. ST Accel. Beams **6**, 044401 (2003).

[39] S. I. Tzenov and R. C. Davidson, Phys. Rev. ST Accel. Beams **5**, 021001 (2002).

[40] I. Hofmann, Z. Naturforsch. **37A**, 939 (1982).

[41] I. Hofmann, Laser Part. Beams **3**, 1 (1985).

[42] O. Boine-Frankenheim, I. Hofmann, and G. Rumulo, Phys. Rev. Lett. **82**, 3256 (1999).

[43] L. K. Spentzouris, J.-F. Ostiguy, and P. L. Colestock, Phys. Rev. Lett. **76**, 620 (1996).

[44] L. K. Spentzouris, P. L. Colestock, and C. Bhat, in *Proceedings of the 1999 Particle Accelerator Conference, New York* (IEEE, Piscataway, NJ, 1999), Vol. 1, p. 114.

[45] R. Fedele, G. Miele, L. Palumbo, and V. G. Vaccaro, Phys. Lett. A **179**, 407 (1993).

[46] H. Schamel, Phys. Rev. Lett. **79**, 2811 (1997).

[47] H. Schamel and R. Fedele, Phys. Plasmas **7**, 3421 (2000).

[48] A. Hofmann, CERN Report No. 77-13, 1977.

[49] D. Neuffer, Part. Accel. **11**, 23 (1980).

[50] C. K. Allen, N. Brown, and M. Reiser, Part. Accel. **45**, 149 (1994).

[51] W. M. Sharp, A. Friedman, and D. P. Grote, Fusion Eng. Des. **32**, 201 (1996).

[52] J. G. Wang, H. Suk, and M. Reiser, Phys. Rev. Lett. **72**, 2029 (1994).

[53] See, for example, p. 505 of Ref. [2].

[54] S. Koscielniak, in *Proceedings of the 2001 Particle Accelerator Conference* (IEEE O-7803-7191-2001, 2001), p. 2970.

[55] S. Koscielniak, S. Hancock, and M. Lindroos, Phys. Rev. ST Accel. Beams **4**, 044201 (2001).

[56] R. C. Davidson (to be published).